Combustion and Flame 263 (2024) 113384

Contents lists available at ScienceDirect

Combustion and Flame

journal homepage: www.sciencedirect.com/journal/combustion-and-flame

Impact of heat transfer due to fiber conduction, radiation and convection on the interpretation of experiments with isolated droplets

Mohamad Asrardel, Álvaro Muelas, Taha Poonawala, Javier Ballester *

Laboratory of Fluids Engineering and Energy (LIFEn) - Engineering Research Institute of Aragon (I3A), University of Zaragoza, Calle Maria de Luna, 3, Zaragoza 50018, Spain

ARTICLE INFO

Keywords:
Droplet evaporation
Experimental artifacts
Fiber conduction
Radiative heating
Convection
Microexplosions

ABSTRACT

Isolated droplet setups have been extensively used during the last decades to characterize liquid fuel evaporation and combustion, being considered a reference framework approaching the simplest and idealized (canonical) configuration. However, in many cases, this configuration is affected by different experimental artifacts that may lead to non-negligible deviations from the assumed ideal conditions and must be duly assessed in order to correctly interpret experimental results. The conduction of heat through the support fibers, the absorption of thermal radiation and external convective effects are specifically studied in this work. A theoretical analysis addresses these undesired effects, proposing a dimensionless number for each artifact (*FN, RN, CN*, respectively), accounting each of them for the ratio of the corresponding additional heat input when compared to the canonical case. For moderate values of these heat inputs, a linear correlation is proposed, where the deviation of the droplet evaporation rate from the canonical case (K/K_{can}) can be predicted solely based on *FN, RN* and *CN*. This correlation has been validated for a wide range of conditions using a droplet evaporation model as well as experiments performed on two different test rigs (drop-tube and suspended droplet setups). Such a broad variety of conditions (in terms of initial droplet diameter, size and material of the suspension fibers, fuel, gas temperature, etc.) is considered to provide a unique and novel dataset with a rich assortment of data, ranging from tests very close to the canonical case to experiments where the artifacts completely distorted the evaporation behavior, surging the evaporation rate and even inducing internal bubbling and puffing events. Additional data from the literature was also examined, further supporting the ability of the proposed approach to accurately capture the deviations in terms of evaporation rate due to these artifacts.

1. Introduction

Spray combustion systems for liquid fuels (boilers, furnaces, engines, gas turbines, etc.) are crucial for power generation and transport, but they face challenges like pollution emissions [1] and resource depletion [2]. To design efficient units that meet human health and environmental standards, a thorough investigation of spray and droplet evaporation dynamics is essential. However, due to the complex nature of spray flames in which many droplets coexist and interact while evaporating, it is extremely challenging to accurately characterize droplet evaporation at spray conditions. Thus, the isolated droplet configuration has been the chosen framework in many studies to investigate fuel droplet evaporation characteristics (e.g., [3–7]) as it allows a close control of the conditions and variables involved. In fact, most of the empirical knowledge available on the evaporation and combustion of fuel droplets has been generated in different versions of single-droplet setups and cover widely different aspects, from reference data for pure compounds to the characterization of the evaporation/combustion behavior of real multi-component fuels, the occurrence of bubbling/puffing/micro-explosions, the formation of solid residues, etc. Independently of the purpose, either model validation or phenomenological study, an indispensable condition is that the experimental setup reproduces the canonical configuration normally sought in this type of test (i.e., idealized scenario with perfectly spherical symmetry). Although isolated droplet setups are designed to fulfill that requirement, deviations from ideal conditions may occur and need to be duly accounted for.

The vaporization of an isolated droplet in a convection-free environment is a spherico-symmetrical problem and provides a canonical configuration that greatly facilitates the interpretation of results and the comparison with mathematical models [8]. Namely, the heating and

* Corresponding author at: Fluid Mechanics Group, School of Engineering and Architecture, Calle Maria de Luna, 3; Zaragoza 50018; Spain.
E-mail address: ballester@unizar.es (J. Ballester).

https://doi.org/10.1016/j.combustflame.2024.113384
Received 18 September 2023; Received in revised form 25 January 2024; Accepted 22 February 2024
Available online 2 March 2024

Nomenclature

CN	Convection number $= (\dot{Q}_{cn}/\dot{Q}_{gc})$, [-]
c	Heat capacity, [J kg^{-1} K^{-1}]
d	Diameter, [μm]
$\bar{E}_a$	Radiation absorption efficiency factor, [-]
FN	Fiber number $= (\dot{Q}_{fc}/\dot{Q}_{gc})$, [-]
f	Correction coefficient, [-]
h	Convective heat transfer coefficient, [W m^{-2} K^{-1}]
k	Thermal conductivity, [W m^{-1} K^{-1}]
K	Droplet evaporation rate, [mm^2 s^{-1}]
L_v	Latent heat of vaporization, [J kg^{-1}]
m	Droplet mass, [kg]
n_f	Number of fibers, [-]
Nu	Nusselt number, [-]
$\dot{Q}$	Heat power, [W]
$\dot{Q}''$	Incident heat flux, [W m^{-2}]
$\dot{q}$	Heat power absorbed per unit of volume, [W m^{-3}]
r	Radial coordinate, [m]
RN	Radiation number $= (\dot{Q}_{rd}/\dot{Q}_{gc})$, [-]
t	Time, [s]
T	Temperature, [K]
v	Velocity, [m s^{-1}]
x	Spatial coordinate, [m]

Greek symbols

ε	Emissivity, [-]
ρ	Density, [kg m^{-3}]
σ	Stefan-Boltzmann constant, [kg s^{-3} K^{-4}]
χ_T	Enhancement coefficient for liquid thermal conductivity, [-]
Ω	Solid angle, [Steradian]
$\forall_{net}$	Net droplet volume, [m^3]

Subscripts

0	Initial
b	Boiling
c	Critical
can	Canonical case
fc	Fiber conduction
cn	Forced convection
d	Droplet
exp	Experimental value
f	Fiber
g	Gas phase
gc	Gas conduction at droplet surface in quiescent atmosphere
l	Liquid phase
rd	Radiation
s	Droplet surface
t	Total

evaporation of the droplet are usually assumed to be solely caused by the conduction of heat transferred to the droplet surface, either from a surrounding gas at a higher temperature or from an envelope flame. This simplified configuration provides a convenient reference for comparison with predictive models, comparison among fuels and conditions, or characterization of specific behaviors (swelling, micro-explosions, etc.). However, real implementations usually involve effects not included in this ideal picture, such as heat conduction through the supporting fibers, convective effects or absorption of thermal radiation emitted from solid walls. Since, to the authors' knowledge, most setups are affected by one or several of these 'experimental artifacts', their magnitude needs to be duly assessed in order to correctly interpret and use the results, either for model validation or for describing the evaporation/combustion behaviors of specific fuels or blends.

The study of droplets suspended on fibers is probably the most common method when it comes to the experimental characterization of these behaviors. Besides its relative simplicity and close control of conditions, this setup is compatible with any type of fuel, including high-viscosity liquids, and allows recording the full history of an individual droplet. However, the conduction of heat through the supporting fibers can cause some departure from the assumed canonical configuration. Its magnitude depends on many variables, including (but not only) the size and material of the fibers. Fiber diameters between 10 and 300 μm and different materials, like quartz [3,4,6], silicon carbide [3,9,10], or thermocouple wires [7], have been used in published works. Some studies have specifically analyzed the magnitude of this 'fiber conduction artifact' and found that, although it is of little importance in some cases, this effect can lead to largely overestimating the evaporation rate (even doubling its true value [3]) or even to artificially induce bubbling or micro-explosions which do not occur for unsuspended, spray droplets [11,12].

Chauveau et al. [3] examined the heat conduction through fibers on n-heptane droplets under various conditions (gas temperature, fiber sizes, etc.), suggesting a crossed configuration of 14 μm silicon carbide (SiC) fibers to mitigate this effect. Moreover, a linear relationship between the measured droplet's evaporation rate and the square of the fiber diameter was found. Similarly, Wang et al. [11] observed the same trend when they explored the influence of ambient temperature (673 K - 973 K) and fibers' properties (k_f and d_f) on the evaporation rate of jatropha methyl ester droplets. Furthermore, they observed micro-explosions occurring for fuel droplets when d_f and k_f exceed 150 μm and 400 W/m/K, respectively. They concluded that a suspension fiber with $d_f < 100$ μm and $k_f < 80$ W/m/K has negligible impact on droplet evaporation rate. Yang and Wong [4] studied the same effect on n-heptane and n-hexadecane droplets, using different suspension fiber diameters, ambient temperatures and initial droplet sizes. The impact of

Novelty and significance statement

Isolated droplet setups constitute an essential source of reference data on the evaporation and combustion processes of liquid fuels. However, departure from ideal conditions due to undesired experimental artifacts may significantly increase the heat input to the droplet (and therefore the evaporation rate) with respect to the assumed canonical scenario. This work thoroughly reviews available knowledge and proposes a novel, comprehensive approach to analyze the impact of those effects. The problem is formulated in terms of easily calculable dimensionless numbers, which allow estimating the magnitude of experimental artifacts: heat conduction through the support fibers, absorption of thermal radiation and convective effects. The method has been thoroughly validated with experimental and modeling results for a wide range of conditions and is expected to constitute a novel, valid framework that can help to correctly interpret test data and to select conditions that minimize or limit the impact of the various experimental artifacts.

fiber-induced heat transfer was reported to also depend on the initial droplet size. Namely, they observed an inverse correlation between the d_0/d_f ratio and the droplet evaporation rate (K), recommending the use a single quartz fiber with $d_f = 50$ μm to minimize fiber conduction effects. Han et al. [7] studied the evaporation of n-dodecane and n-hexadecane droplets suspended at thermocouple wires and quartz fibers. They found that using a thermocouple as the suspension medium can significantly increase droplet evaporation rate, as also reported by previous works [8]. Setyawan et al. [13,14] investigated the combustion of pure glycerol suspended on a 142 μm SiC fiber, noting unexpected fluctuations in the evaporation curve. Since pure glycerol should evaporate smoothly without any puffing, the observed bubbling suggests heterogeneous nucleation at the hot fiber surface [12]. Farouk and Dryer [9] conducted a numerical study on the impact of fiber properties (k_f and d_f) on n-decane droplet combustion. For d_f =45 μm SiC rod arrangements, they recommended d_0/d_f >38 as a safe criterion to minimize this fiber conduction effect. In the same line, Avedisian and Jackson [15] recommended d_0/d_f >13 to mitigate the impact of a suspending quartz fiber on the burning rate of n-heptane, recovering the burning rate of a fiber-free droplet. As it can be noticed, the recommended criteria proposed in previous works to avoid the fiber conduction artifact are quite diverse and, in some cases, even contradictory.

Heat transfer to the droplet (and therefore evaporation rate) can also be increased by the presence of hot radiating surfaces near the droplet. Obviously, this is not a problem if this additional heat source is an objective of the test or, at least, it is duly considered; otherwise, this 'radiation artifact' may lead to overestimating the evaporation rate with respect to the true value for the canonical case. The effect of thermal radiation absorption on the droplet evaporation process was analyzed by Fang et al. in [16], concluding that radiation effects can become considerable at high temperatures, significantly decreasing the droplet lifetime. Long et al. [17] modeled the effect of radiation absorption for different ambient temperatures and found that there is a critical droplet diameter below which the impact of radiation absorption can be assumed negligible. Gan and Qiao [18] quantified the evaporation rates of ethanol droplets (both pure and with nanoparticles) exposed to different levels of radiation heat flux at room temperature. They observed an increase of 12.4 % in evaporation rate for ethanol when the radiation level of a mercury lamp was raised from 75 to 175 W. All these studies confirm that radiation effects should be duly accounted for in order to correctly interpret experimental results on droplet evaporation.

Gas-droplet heat exchange, and hence evaporation rate, can also be enhanced due to forced or natural convection. Buoyancy-free conditions can only be fully achieved under microgravity [19]. Otherwise, depending on the experimental conditions (e.g., droplet size), buoyancy-induced flows can noticeably enhance the evaporation rate compared to the canonical problem [3]. However, most literature data on droplet evaporation relies on tests performed under normal gravity. If the droplet is not in a stagnant ambient, forced convection may also enhance the evaporation rate, as it can be readily estimated through the Nusselt number [20].

This brief survey demonstrates that artifacts due to departures from canonical conditions may cause deviations that can widely exceed acceptable uncertainties, for example, in terms of evaporation rate in model validation exercises or when comparing data from different sources, conditions, or fuels. Some previous works provide valuable analyses and hints, but they focused on particular conditions and are difficult to generalize to other situations. This work aims to quantify and parameterize the aforementioned experimental artifacts in a global manner. A dimensionless analysis is proposed in order to determine the relevant parameters and magnitudes of the different experimental artifacts. This analysis, combined with droplet evaporation modeling, is applied to experimental data from two different facilities (suspended and free-falling droplets) as well as to some published data, proving its usefulness to capture deviations in evaporation rate due to these artifacts for a wide range of conditions.

2. Experimental and predictive methods

2.1. Experimental facilities

Two types of isolated droplet setups are used in this study: a drop tube (DCF) and a suspended droplet facility (SDF). In the former, a train of isolated droplets (d_0=145 μm) is generated by a piezoelectric device and injected into a cylindrical combustion chamber. The monodisperse droplets evaporate while falling along the axis of a hot gas coflow (average T_g of 1730 K [5]) provided by a premixed, flat-flame McKenna burner. The coflow is directed downwards, so that the gas-droplet relative velocity is reduced (Reynolds number ~0.2 during most of the droplet vaporization history). The radiative heat flux inside the cylindrical combustion chamber was measured with an ellipsoidal radiometer probe [21], yielding values in the interval 29.4 - 20.6 kW/m^2 at axial distances from the burner surface of 30 and 90 mm, respectively. The repetition of a given experiment in this facility was found to provide deviations in quasi-steady evaporation rate of 0.7 % [5]. More details about the DCF setup can be found in [5].

As for the SDF setup, it uses significantly bigger droplets (d_0 = 350 - 1200 μm), which are anchored by different suspension arrangements. In this work, Nicalon™ silicon carbide (d_f = 15 μm), Nextel® 312 Al/Si/B (d_f = 11 μm), quartz (d_f = 100 μm) fibers and platinum wires (d_f = 25 and 50 μm) are used as suspension medium. Different fiber arrangements are considered for this study. A cross-fiber arrangement was used for SiC and Al/Si/B, consisting of two single fibers (2 × 1) or two bundles of 3 or 6 fibers each (2 × 3, 2 × 6). In the case of Pt25, Pt50, and quartz, the fuel droplet is suspended from a single filament (U-shaped in the case of Pt wires). Fig. 1 displays a schematic of SDF and its different parts.

The high-temperature environment is provided by a premixed, flat-flame McKenna burner which, similarly to the DCF, is adjusted to yield oxygen-free combustion products. A quartz tube confines the hot gas flow, directed downwards. Gas velocity measurements demonstrated that it was always below 0.1 m/s, which leads to a Reynolds number <0.5 during the lifetime of 500 μm droplets. Initially, the fuel droplet is protected against the downward hot gas flow from the burner by a horizontal flat cold air jet, which maintains the temperature at the droplet location at ~325±1 K, until the test starts. After the triggering signal is initiated, the camera acquisition starts, and the cold air jet is interrupted, exposing the fuel droplet to the hot gas flow. The temperature rise is measured with a 75 μm bare S-type thermocouple, showing a very repeatable temperature record slightly increasing with time, so that the droplet completely evaporates in an ambient temperature range of 1336 ± 50 K. The radiative heat flux at the droplet location, as measured with an ellipsoidal radiometer, is 23.5 kW/m^2. A high-speed camera (Chronos 2.1) is used to acquire backlit images of the fuel droplet evaporation process at 1000 fps and 1-Mpx resolution. The images collected by the camera are later processed in Matlab® in order to automatically extract the temporal evolution of the droplet size. Repeating a given experiment in this facility (butanol droplet suspended by two SiC fibers, d_0=500 μm) was found to yield a relative standard deviation of 0.9 % in terms of quasi-steady evaporation rate for the twelve tested runs.

The experiments at both facilities were performed with two pure compounds of well-known physico-chemical and transport properties: n-butanol and glycerol. Since the droplet evaporation process is studied under high-temperature conditions, alcohols were chosen to avoid the potential influence of gas-phase thermal decomposition reactions [22]. Among the alcohol chemical family, butanol and glycerol were chosen due to their widely different properties.

2.2. Droplet evaporation model

To emulate the isolated fuel droplet vaporization at high temperatures and to assess the effects of different experimental artifacts on the evaporation characteristics, a 1-D model has been developed based on

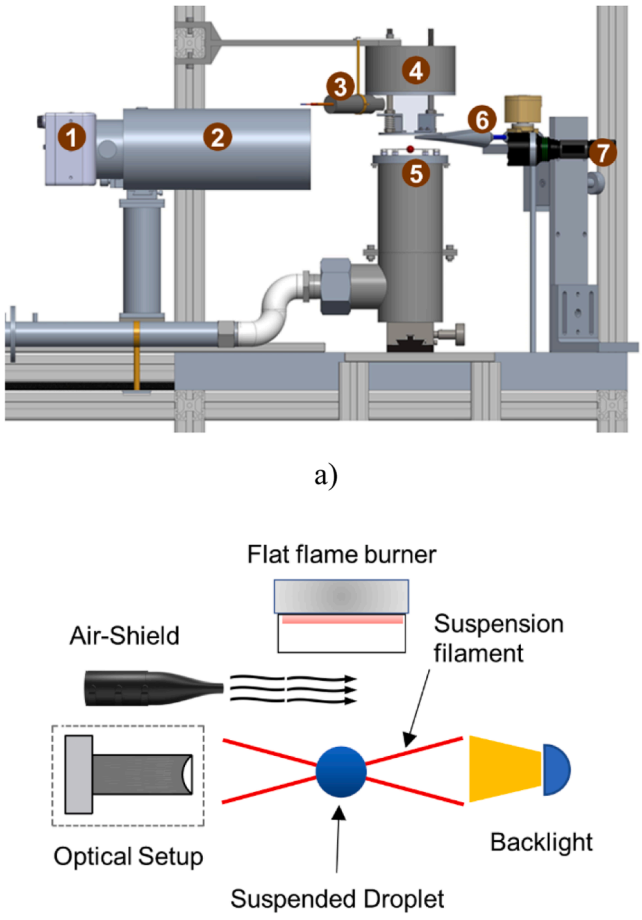

Fig. 1. Schematic of the suspended droplet facility. a) 3-D view: 1 camera, 2 lens, 3 flame monitoring device, 4 McKenna burner, 5 Suspended droplet, 6 Air-shield, and 7 Backlight. b) 2-D, simplified side view.

the Abramzon-Sirignano droplet evaporation model [20]. The model has been thoroughly validated in previous works, yielding excellent agreement with DCF data for the two alcohols tested in this study (e.g., see [22]).

Although the Reynolds numbers at both facilities are quite reduced, the model takes into account the effects of enhanced heat and mass transfer caused by forced convection employing the correlations proposed in [20]. The energy equation for the liquid has been modified to include additional heat flows due to conduction through the fiber ($\dot{q}_{fc}$) and radiation ($\dot{q}_{rd}$), following the approaches proposed in [23,24]. Eq. (1) shows the final form for the liquid energy equation with those two heat source terms, assumed to be uniformly distributed within the droplet volume.

$$\rho_l c_l \frac{\partial T_l}{\partial t} = \frac{1}{r^2}\frac{\partial}{\partial r}\left(\chi_T k_l r^2 \frac{\partial T_l}{\partial r}\right) + \dot{q}_{fc} + \dot{q}_{rd} \tag{1}$$

The heat absorbed by conduction through the fiber can be estimated by solving the 1-D heat equation along the fiber (see Eq. (2)) [23]

$$\begin{aligned} x > \frac{d_d}{2}: \ \rho_f c_f \frac{\partial T_f}{\partial t} &= k_f \frac{\partial^2 T_f}{\partial x^2} + \frac{4h_g}{d_f}\left(T_g - T_f\right) - \frac{4\varepsilon_f}{d_f}\left(\sigma T_f^4 - \frac{\dot{Q}_{rd}^{''}}{4\pi}\right) \\ x < \frac{d_d}{2}: \ \rho_f c_f \frac{\partial T_f}{\partial t} &= k_f \frac{\partial^2 T_f}{\partial x^2} + \frac{4h_l}{d_f}\left(T_l - T_f\right) \end{aligned} \tag{2}$$

h_g and h_l are the heat convection coefficients in the parts of the fiber in contact with gas and liquid, respectively, estimated as $h_g = Nu_g k_g/d_f$ and, $h_l = Nu_l k_l/d_f$. The Nusselt number is calculated with the correlations for cylinders recommended in [25,26]. The fiber is assumed to act as a grey-body, with an emissivity (ε_f) adopted from [27], receiving radiation over a solid angle Ω (Ω=2π for SDF and DCF tests, since radiation only comes from the upper hemisphere). Incident thermal radiation heat flux ($\dot{Q}_{rd}^{''}$) is set according to the measurements performed at both facilities: 23.5 kW/m^2 for SDF and 20.6 - 29.4 kW/m^2 for DCF. The physical properties of SiC, Al/Si/B, Pt, and quartz are adopted from [23, 28-30].

Once the temperature distribution along the fiber is obtained, the fiber conduction heat absorbed by the droplet can be estimated as [31]:

$$\dot{q}_{fc} = \left(\int_{x=-r}^{x=+r} h_l(x)\left(T_l(x) - T_f(x)\right)\pi d_f n_f dx\right) \Big/ \forall_{net} \tag{3}$$

The modeling of the droplet radiative heating features a wide range of possible approaches, as detailed in [32]. In the current work, the radiation source term in Eq. (1), $\dot{q}_{rd}$, is calculated as:

$$\dot{q}_{rd} = \pi {d_d}^2 \frac{\Omega_d}{4\pi} \bar{E}_a \dot{Q}_{rd}^{''} \Big/ \forall_{net} \tag{4}$$

Splitting therefore the estimation of the heat absorbed by the droplet ($\dot{q}_{rd}$) into its different contributing factors: the radiative heat flux ($\dot{Q}_{rd}^{''}$, which can be either experimentally measured or estimated through different approaches), the effective area receiving this flux ($\pi {d_d}^2 \frac{\Omega_d}{4\pi}$) and, finally, the fraction of the heat impacting the droplet which is absorbed ($\bar{E}_a$). Since $\dot{q}_{rd}$ is expressed in volumetric basis, the resulting absorbed heat is divided by the net volume of liquid. Further details regarding Eq. (4) can be found in Appendix A of the Supplementary materials.

3. Experimental results

The evaporation of butanol and glycerol droplets has been studied at the suspended droplet facility (SDF) with different configurations and conditions. As described in Section 2, the droplets were suspended on different arrangements: cross-fiber configurations 2 × 1 (2 fibers, SiC and Al/Si/B), 2 × 3 (6 fibers, SiC), and 2 × 6 (12 fibers, SiC), as well as single filaments of quartz and platinum. Fig. 2 displays the experimental evaporation curves for butanol and glycerol droplets with an initial diameter of d_0=500 μm suspended on these arrangements. The slope of this curve in its linear region (d^2/d_0^2 = 0.2 - 0.6) is denoted as the average, quasi-steady evaporation rate (K=-d(d^2)/dt [mm^2/s]), indicated in the legends. In theory, if the fibers had no significant effect, all the curves and K values should be about the same. On the contrary, Fig. 2 reveals large differences among curves, clearly demonstrating a significant influence of the suspension medium on the evaporation behavior, with noticeably higher evaporation rates and shorter droplet consumption times for thicker fiber arrangements. The curves for platinum wires show some erratic behaviors that will be discussed later on.

The dashed curves in Fig. 2 are model predictions for unsuspended droplets. The model has been thoroughly validated with data from the DCF (deviations <3 % in K for both butanol and glycerol [22]) and therefore, is expected to provide a good estimate of the size evolution for the canonical case, i.e., without any experimental artifact. The fact that these predictions are closer to the cases with thinner fibers (2 × 1, both SiC and Al/Si/B) is fully consistent with heat conduction through the supporting filaments artificially accelerating the evaporation process.

Fig. 3 displays the quasi-steady evaporation rate obtained in 249 different experiments conducted at SDF as a function of the initial droplet size. These experiments encompass a wide range of conditions, with different droplet sizes (d_0) and fiber arrangements (diameter, conductivity, and number of fibers: d_f, k_f, n_f), using butanol (T_b = 390 K) and glycerol (T_b = 563 K) as fuels. The evaporation rate calculated for

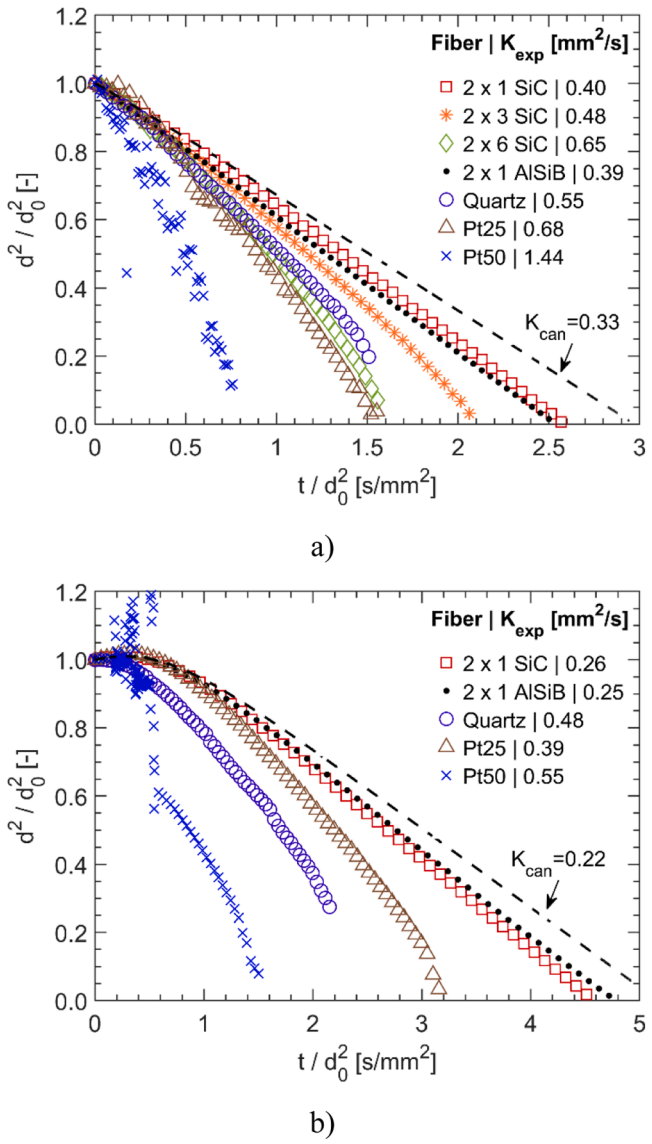

Fig. 2. Experimental evaporation curves for fuel droplets suspended at different fiber arrangements. a) butanol, b) glycerol. The dashed lines represent model predictions for the canonical case.

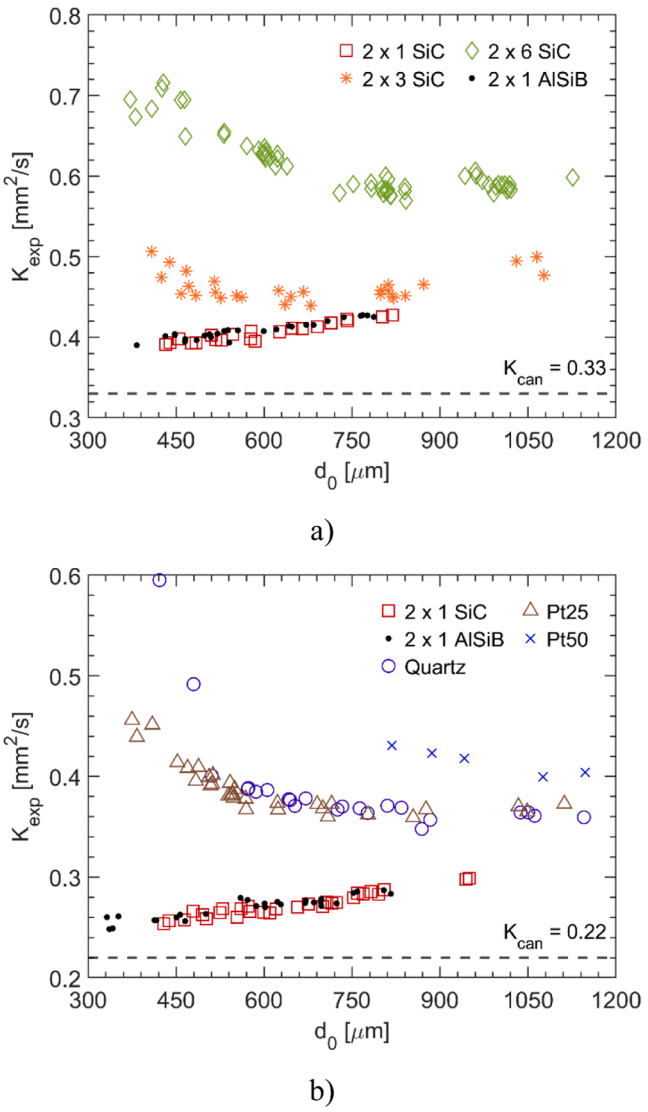

Fig. 3. Evaporation rate measured for fuel droplets vs. initial droplet size, with different fiber arrangements at SDF experiments. Dashed line: predicted canonical value (K_{can}) by modeling. a) butanol, b) glycerol.

the canonical case (free droplet without radiation or convective effects), K_{can}, is also represented and, in agreement with theory, does not vary with d_0.

In all cases, $K_{exp} > K_{can}$, with large differences (even exceeding 2 ×) in some of the tests, which can only be attributed to the artifacts occurring in the SDF experiments. Thus, it is clear that $\Delta K = K_{exp} - K_{can}$ strongly depends on test conditions. As already discussed, fiber conduction can significantly enhance the heat input to the droplet (and therefore K_{exp}) and is a function of the fiber size and material. This can explain the differences among the various test series, with ΔK increasing with the number, size and conductivity of the fibers. However, other effects are not so obvious, such as the fact that ΔK either increases or decreases with droplet size, d_0, depending on other test conditions. This must be due to the combination of different causes: fiber conduction, radiation, and convective effects. Droplets with larger d_0 expose a greater surface area, thereby increasing their capacity to receive radiative heat. In addition, an increase in d_0 also results in higher Grashof and Reynolds numbers ($Gr \propto d_0^3$ and $Re \propto d_0$) for the surrounding hot gas flow, leading to an augmented heat transfer from the hot gas through natural [33] and forced convection mechanisms [34]. Both effects would justify an increase in K_{exp} with d_0, but this only occurs when the effect of the fiber is sufficiently small (i.e., 2 × 1 SiC or Al/Si/B fibers). Cases with a larger number of fibers and/or thicker filaments show the opposite behavior, with K_{exp} decreasing with d_0. This is ascribed to the reduced impact of the fiber for sufficiently large droplet sizes, in agreement with previous works which suggested the relevance of the d_0/d_f ratio [4,15]. All three potential artifacts must be considered in order to explain the experimental observations for a particular case. This is attempted in the analysis presented in Section 4.

Some of the tests with droplets suspended on Pt wires reveal a distinct behavior, both for butanol (d_f =25 and 50 μm) and glycerol (d_f =50 μm), with sudden fluctuations in droplet size (see Fig. 2) due to the occurrence of internal bubbling and puffing events, occasionally accompanied by weak micro-explosions. Fig. 4 shows a series of images captured at different time intervals during the evaporation of a butanol droplet suspended on a 50 μm platinum wire. The formation of bubbles within the liquid begins and gradually expands (Fig. 4b), causing the surface of the droplet to wrinkle and exhibit puffing behaviors (Fig. 4c). At certain moments, the swelling of the droplet becomes more pronounced, leading to the ejection of tiny droplets with significant velocity from the droplet surface (Fig. 4d). These puffing events have been

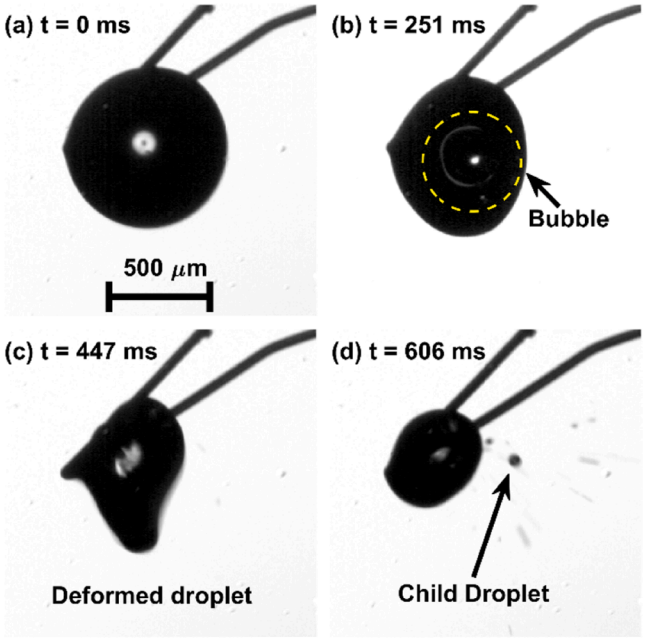

Fig. 4. Different instances during SDF evaporation tests of a butanol droplet suspended on a 50 μm platinum wire (Pt50).

previously reported by Wang et al. [11] and can be considered as a strong distortion of the droplet evaporation process. This behavior is ascribed to a very strong fiber conduction effect, favored by the high thermal conductivity of Pt and the relatively large filament cross-section. As a result, the fiber temperature increases above the liquid boiling temperature, creating hotspots where vapor nucleation can occur [11]. This phenomenon leads to significant deviations from the quasi-steady linear surface regression characteristic of a single-component fuel droplet and, therefore, the experimental results obtained under such conditions are no longer a valid description of its real evaporation characteristics.

These artifacts were observed for droplets suspended on platinum and quartz filaments, but their occurrence and intensity varied among tests, as summarized in Table 1. The tendency to form bubbles was higher for butanol than for glycerol, decreased with droplet size, and resulted in more intense puffing for platinum than for quartz. For 15 μm SiC fibers, evaporation took place smoothly in all cases, with the only exception of tests with 500 μm butanol droplets, where some bubbling appeared but only at the very end of their lifetime (e.g., in one case it started when the droplet size fell below 58 μm). So, it is not possible to propose simple rules to predict the onset of these artifacts, since they depend on the particular combination of experimental conditions. The formation of bubbles requires reaching nucleation conditions at some locations inside the droplet, which depends on both heat transfer through the fiber and liquid properties.

In order to further explore this hypothesis, the temperature profile along the fiber was calculated with the model described above for different test conditions. The results are shown in Fig. 5, in terms of the average temperature of the fiber in the portion inside the droplet, $\bar{T}_f$. As a reference, the critical temperatures for butanol and glycerol are indicated. Vapor nucleation is expected to occur when the liquid reaches its superheating temperature, typically around 90 % of T_c [35], so the critical temperature can be used as a valid reference to assess bubble formation. The results in Fig. 5 are fully consistent with the experimental observations summarized in Table 1. With butanol, the fiber temperature widely exceeds its critical temperature for both Pt wires, and also reaches T_c at the very end of the droplet lifetime for SiC fibers. For glycerol, this only clearly happens for Pt-50, whereas for Pt-25 (for which no bubbling was observed) the critical temperature is only exceeded during the final instants of the evaporation process.

This simple analysis clearly demonstrates that the thermal disturbance due to the fiber can explain abnormal behaviors (bubbling or even micro-explosions for monocomponent droplets) that significantly modify the actual evaporation process of the liquid under study and, hence, must be avoided. Since it is not possible to obtain a valid evaporation rate from tests showing these experimental artifacts, they will not be further considered for subsequent analysis in the following sections.

Table 1
Occurrence of puffing or bubbling events for different fuels and conditions.

Fuel	d_0	Pt - 25μm	Pt - 50μm	Quartz - 100μm
Butanol	450 μm	Puffing	Puffing	Bubbling
	800 μm	Puffing	Puffing	Bubbling
Glycerol	450 μm	No	Micro-explosion	No
	800 μm	No	Puffing	No
	1076 μm	N/A	No	N/A

4. Theoretical analysis of the artifacts

This section intends to evaluate and parameterize the impact of each experimental artifact by introducing a simplified analysis based on global characteristic parameters of the problem of an isolated droplet evaporating within a high-temperature gas coflow.

Droplet evaporation is driven by the total heat transferred to the liquid, $\dot{Q}_t$. Assuming that the droplet vaporizes under the quasi-steady regime, where all the heat input to the droplet is used to evaporate, it can be stated that:

$$K \sim \frac{\dot{Q}_t}{mL_v} = \frac{\dot{Q}_{gc} + \dot{Q}_{fc} + \dot{Q}_{rd} + \dot{Q}_{cn}}{mL_v} = \frac{\dot{Q}_{gc}}{mL_v}\left(1 + \frac{\dot{Q}_{fc}}{\dot{Q}_{gc}} + \frac{\dot{Q}_{rd}}{\dot{Q}_{gc}} + \frac{\dot{Q}_{cn}}{\dot{Q}_{gc}}\right) \quad (5)$$

Where $\dot{Q}_t$ is decomposed into the possible heat transfer modes: conduction of heat through the gas-liquid interface ($\dot{Q}_{gc}$) and through the fiber-liquid interface ($\dot{Q}_{fc}$), absorption of radiative heat ($\dot{Q}_{rd}$) and the excess heat input due to convection with respect to conduction in stagnant conditions ($\dot{Q}_{cn}$). $\dot{Q}_{gc}$ is the only heat transfer mechanism intrinsic to the canonical problem, so that the evaporation rate in those idealized conditions, K_{can}, is proportional to $\dot{Q}_{gc}$:

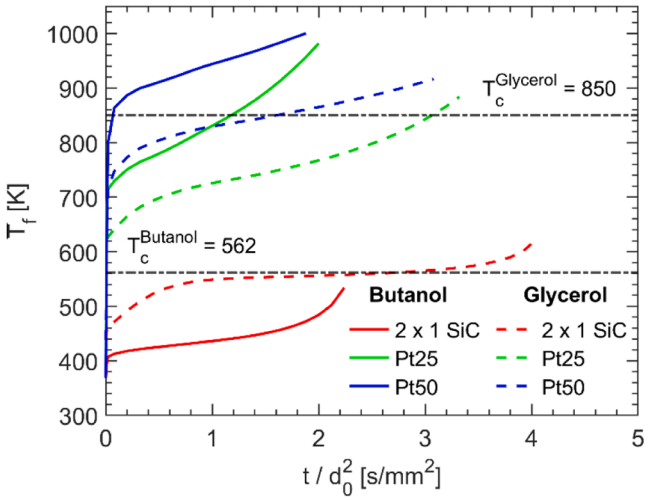

Fig. 5. Predicted temporal evolution of the average temperature of the fiber inside the droplet for butanol (solid lines) and glycerol (dashed lines) for different fiber arrangements and $d_0 = 800\mu m$.

$$K_{can} \sim \frac{\dot{Q}_{gc}}{mL_v} \tag{6}$$

The rest of the terms in Eq. (5) are due to additional heat transfer modes, leading to deviations from an idealized configuration in which only $\dot{Q}_{gc}$ exists. Those deviations in real setups can be interpreted as experimental artifacts, resulting in a deviation in evaporation rate, $\Delta K = K - K_{can}$, which depends on the relative importance of the various heat transfer mechanisms compared to $\dot{Q}_{gc}$. Since the exact relationship is not necessarily known, Eq. (5) can be reformulated as:

$$\begin{aligned} K &= K_{can} + \Delta K\left(\frac{\dot{Q}_{fc}}{\dot{Q}_{gc}}, \frac{\dot{Q}_{rd}}{\dot{Q}_{gc}}, \frac{\dot{Q}_{cn}}{\dot{Q}_{gc}}\right) \\ K &= K_{can} + \Delta K(FN,\ RN,\ CN) \end{aligned} \tag{7}$$

where *FN, RN* and *CN* are dimensionless numbers related to the fiber conduction, radiation and convective effects, respectively.

Eq. (7) postulates that K and the deviation with respect to K_{can} due to the extra heat transfer modes, ΔK, depend on the dimensionless numbers *FN, RN* and *CN*, without presuming any specific functional form. Furthermore, with some simplifying assumptions, according to Eq. (5), a second postulate is that K and ΔK might admit an additive solution as a direct sum of the three proposed dimensionless numbers:

$$\begin{aligned} \Delta K(FN,\ RN,\ CN)/K_{can} &= FN + RN + CN \\ K/K_{can} &= 1 + \Delta K/K_{can} = 1 + FN + RN + CN \end{aligned} \tag{8}$$

Obviously, this is only strictly valid if the heat transfer modes admit superposition (expected to occur only for small departures from ideal conditions).

Eqs. (7) and (8) may provide a useful framework to assess the magnitude of experimental artifacts as well as to identify the role of the different variables. The objective now is to prove if these expressions correctly describe the importance and trends of experimental artifacts due to the additional heat transfer mechanisms, for conditions representative of those normally encountered in isolated droplet experiments. To that end, an order of magnitude analysis is proposed to express heat transfer rates and the associated dimensionless numbers as a function of the relevant variables.

The conduction of heat through the gas-liquid interface can be readily estimated from the classical theory of droplet evaporation. If the droplet is assumed to vaporize at its boiling temperature (valid for $T_g \gg T_b$), and the Stefan flow is neglected:

$$\dot{Q}_{gc} = \pi d_d Nu_{d,can} k_g \left(T_g - T_b\right) \tag{9}$$

Being $Nu_{d,can}$ the Nusselt number for a stationary droplet immersed in a stagnant flow ($Nu_{d,can}$=2) [4]. It is worth noting that the aim of this simplified analysis is to parameterize the problem based on characteristic parameters of the problem. More accurate estimations for $\dot{Q}_{gc}$ are naturally possible, but the dependence on characteristic, known variables would be lost. Thus, even if Eq. (9) can yield significant errors for high Spalding number cases, its use in this order of magnitude analysis is considered adequate.

The heat transferred to the droplet due to fiber-liquid conduction, $\dot{Q}_{fc}$, can be calculated as the heat flow through the fiber cross-section at the droplet surface:

$$\dot{Q}_{fc} = 2\, n_f \left(\frac{\pi}{4} d_f^2\right) k_f \left.\frac{dT_f}{dr}\right|_s \tag{10}$$

In agreement with previous works [36], this heat scales with the fiber diameter squared and the fiber conductivity. In order to obtain $\dot{Q}_{fc}$, a good estimate of the fiber temperature gradient at the droplet surface is required. This can be readily and accurately calculated by means of models such as the one described in Section 2.2. However, with some simplifications, the required temperature gradient can also be estimated from the global parameters of the problem. For sufficiently thin fibers ($d_f << d_d$), the fiber can be approximated as a fin with $T_f \approx T_b$ at its base ($x = 0$), in a flow at T_g. According to the pin fin theory [37], the temperature profile along the fiber is:

$$T_f(x) = T_g + \left(T_b - T_g\right) \exp\left(- \sqrt{4\, Nu_f \frac{k_g}{k_f}}\ \frac{x}{d_f} \right) \tag{11}$$

For negligible velocity of the hot gas, the fiber Nusselt number is $Nu_f = 0.3$ [25]. From Eq. (11), the thermal gradient at the surface can be readily obtained, yielding the following expression for $\dot{Q}_{fc}$:

$$\dot{Q}_{fc} = 2\, n_f \left(\frac{\pi}{4} d_f^2\right) k_f \frac{\left(T_g - T_b\right)}{\sqrt{\frac{k_f}{k_g} \frac{1}{4\, Nu_f}}\, d_f} \tag{12}$$

Therefore, the dimensionless number *FN* accounting for the effect of the conduction through fibers on the droplet evaporation rate can be calculated as:

$$FN = \frac{\dot{Q}_{fc}}{\dot{Q}_{gc}} = n_f \frac{d_f}{d_d} \sqrt{\frac{k_f}{k_g}}\ \frac{\sqrt{Nu_f}}{Nu_{d,can}} \tag{13}$$

The heat input due to radiation absorption ($\dot{Q}_{rd}$) can be estimated from average values for the incident thermal radiative heat flux ($\dot{Q}_r^{''}$) and the radiation absorption efficiency factor ($\bar{E}_a$). If the droplet sees the radiation source under a solid angle Ω_d and neglecting the radiative emission from the liquid droplet (since $T_g >> T_b$), the resulting heat input to the droplet becomes:

$$\dot{Q}_{rd} = \pi\, d_d^2\, \bar{E}_a \frac{\Omega_d}{4\pi} \dot{Q}_r^{''} \tag{14}$$

The dimensionless *RN* can be therefore estimated as:

$$RN = \frac{\dot{Q}_{rd}}{\dot{Q}_{gc}} = \frac{d_d \bar{E}_a \frac{\Omega_d}{4\pi} \dot{Q}_r^{''}}{Nu_{d,can} k_g \left(T_g - T_b\right)} \tag{15}$$

The case of the last additional heat transfer mechanism (convective effects) is quite straightforward. The ratio of the heat input to the droplet due to convection ($\dot{Q}_{cn}$) and the heat input due to gas-liquid conduction ($\dot{Q}_{gc}$) can be simply expressed in terms of the droplet Nusselt number. Therefore, *CN* can be defined as:

$$CN = \frac{\dot{Q}_{cn}}{\dot{Q}_{gc}} = \frac{Nu_d - Nu_{d,can}}{Nu_{d,can}} = \frac{Nu_d}{2} - 1 \tag{16}$$

In this manner, the three proposed dimensionless numbers can be readily calculated based on global characteristic parameters of the problem, allowing a simple estimation of the impact of each experimental artifact on the droplet evaporation rate.

5. Analysis and evaluation of the artifacts

The magnitude of the different artifacts is now evaluated under a wide range of conditions, while also assessing the capability of the proposed simplified approach to capture their effects on the droplet evaporation behavior. To that end, this section will make use of both model predictions and experimental data.

5.1. Analysis based on model predictions

The model presented in Section 2.2 can be used to evaluate the individual effect of each artifact on the droplet evaporation process, estimating its relevance for different conditions. For instance, Fig. 6a illustrates the variation of K/K_{can}, as predicted with the model, for butanol droplets attached by a single SiC fiber vaporizing in N_2 at 1400 K, for different fiber and droplet diameters. As expected, K/K_{can} increases with d_f and decreases with d_0, consistently with the relative

importance of the heat transferred through the suspension fiber compared with the heat received through the gas-liquid interface. As it can be seen, even a low-conductivity material fiber like SiC ($k_f = 2$ W/m/K) can significantly enhance the evaporation rate of a 500 μm droplet (by ~20 %) when the fiber size is sufficiently large ($d_f = 60$ μm).

According to [4,9,15], the fiber-to-droplet diameter ratio is a representative quantity for the fiber conduction artifact. This is also confirmed in this study, where all the data in Fig. 6a have been plotted against d_f/d_0 in Fig. 6b and get perfectly aligned along a narrow band (see data for $k_f = 2$ W/m/K). However, the fiber conduction artifact must also vary with the thermal conductivity of the material, as confirmed by the predictions shown in Fig. 6b, showing that the deviation in K consistently increases with k_f.

Similarly, other parameters, like the number of fibers or Nusselt numbers, also modify the relative importance of the different heat transfer modes and should be considered. This is precisely the purpose of FN (Eq. (13)), expressing the ratio between heat conduction through the fiber and at the droplet-gas interface. Fig. 6c represents K/K_{can} as a function of FN for all the test cases analyzed: a total of 116 combinations, including different liquids (butanol and glycerol) and a wide range of gas temperatures (700 and 1400 K), initial droplet size (300 - 800 μm), fiber diameter (1 - 60 μm) and fiber thermal conductivity (2–15 W/m/K). Despite the broad range of conditions considered, all data points collapse in Fig. 6c to depict a very well-defined trend, confirming that ΔK or K/K_{can} can be formulated in terms of the dimensionless numbers proposed here (in this case, FN is the only relevant one) as expressed in Eq. (7). Furthermore, the dependency is practically linear for $FN<0.2$, as predicted in the simplified analysis of Section 4, and quite close to $1+FN$. Actually, the best fit in that interval is obtained for $K/K_{can}=1 + 1.21 \times FN$. The factor 1.21 can be interpreted as a calibration factor to match the actual thermal behavior of the fiber, not perfectly captured in the order-of-magnitude analysis (in particular, the estimate of the temperature gradient from the pin fin theory for uniform gas temperature). Anyway, this appears to be quite a modest correction. As FN increases beyond 0.2, linearity is gradually lost, as could be expected since the addition of heat transfer modes is only valid for small departures from canonical conditions. For large fiber sizes and/or conductivities, the problem becomes far more complex, temperature profiles in the droplet and fiber are no longer 1-D and the solution does not admit superposition. As reported in [7], for sufficiently thick fibers the evaporation rate can even start to decrease, since the fiber heating rate is slower, reducing in that way the heat input to the droplet and K. In any case, the generic formulation expressed by Eq. (7) is clearly confirmed. Furthermore, the linear relationship predicted by Eq. (8) is verified to hold in the region not very far from canonical conditions, where it could be used to estimate or even (at least, in a first approximation) correct evaporation rates obtained from experiments; cases with large FN values will result in larger deviations but, in those cases, rough estimates could be more than enough to assess the magnitude of this experimental artifact.

As for the radiation artifact, Fig. 7a shows the impact of the incident radiative heat flux and initial droplet size on K/K_{can} as predicted for unsuspended droplets. An increasing trend exists between K/K_{can} and d_0 due to a larger effective surface for radiative heat absorption. Obviously, increasing $\dot{Q}_r''$ also enhances the evaporation rate, so that a radiative heat flux of 150 kW/m^2 would increase the evaporation rate of 600 μm droplets by approximately 75 %. Such a thermal radiative heat flux could be perfectly reached in furnaces (e.g., hot walls at 1400 K behaving as a grey body with $\varepsilon = 0.7$), and therefore a careful assessment of this effect should be considered when extracting droplet evaporation characteristics under high-temperature conditions, particularly when using big droplets.

Analogously to the case of fiber conduction, the magnitude of the radiation artifact depends on several parameters. Once again, the simplified approach proposed in Section 4 aims to unify all of them into a single non-dimensional 'radiation number', RN (Eq. (15)). Fig. 7b

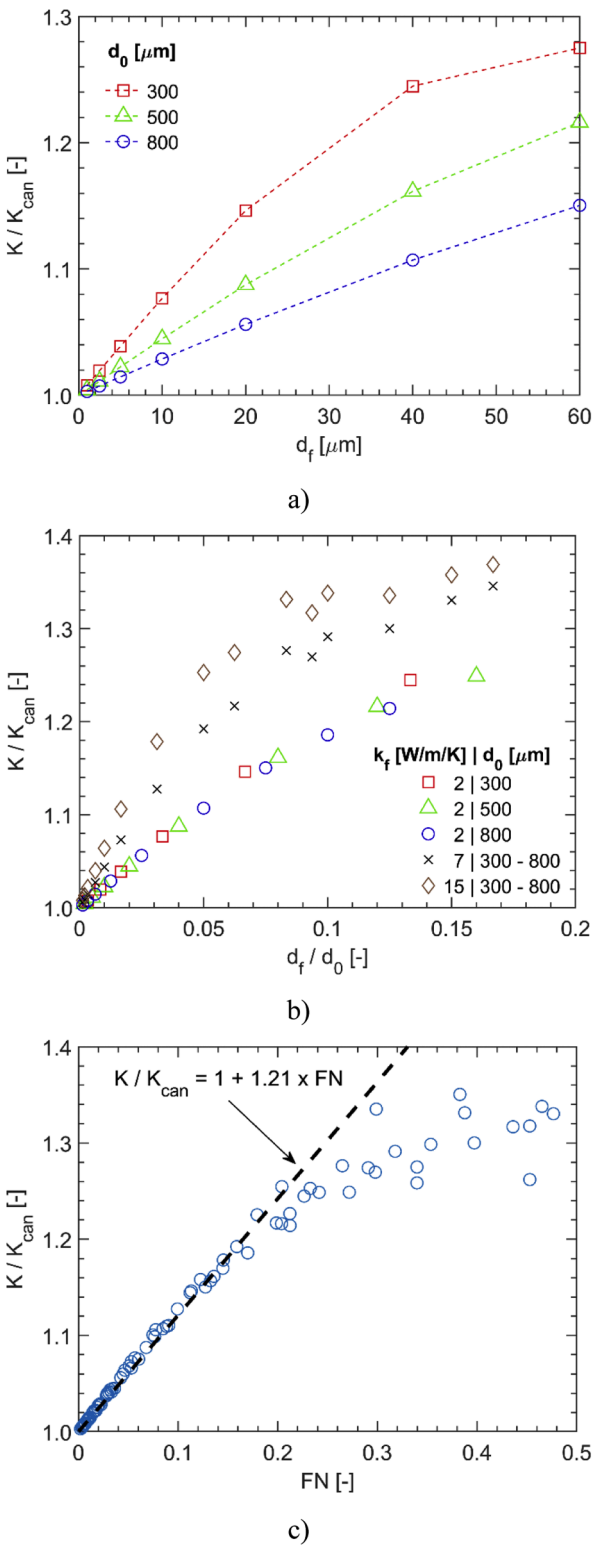

Fig. 6. Calculated K/K_{can} for different droplet and fiber configurations. (a) Effect of d_f and d_0 for butanol droplets suspended on a single SiC fiber, $T_g = 1400$ K; (b) K/K_{can} as a function of d_f/d_0 for butanol and different fiber conductivities, $T_g = 1400$ K. (c) K/K_{can} vs. FN for a wide range of conditions: butanol and glycerol, $T_g = 700$ - 1400 K, $d_f = 1$ - 60 μm, $d_0 = 300$ - 800 μm, $k_f = 2$ - 15 W/m/K.

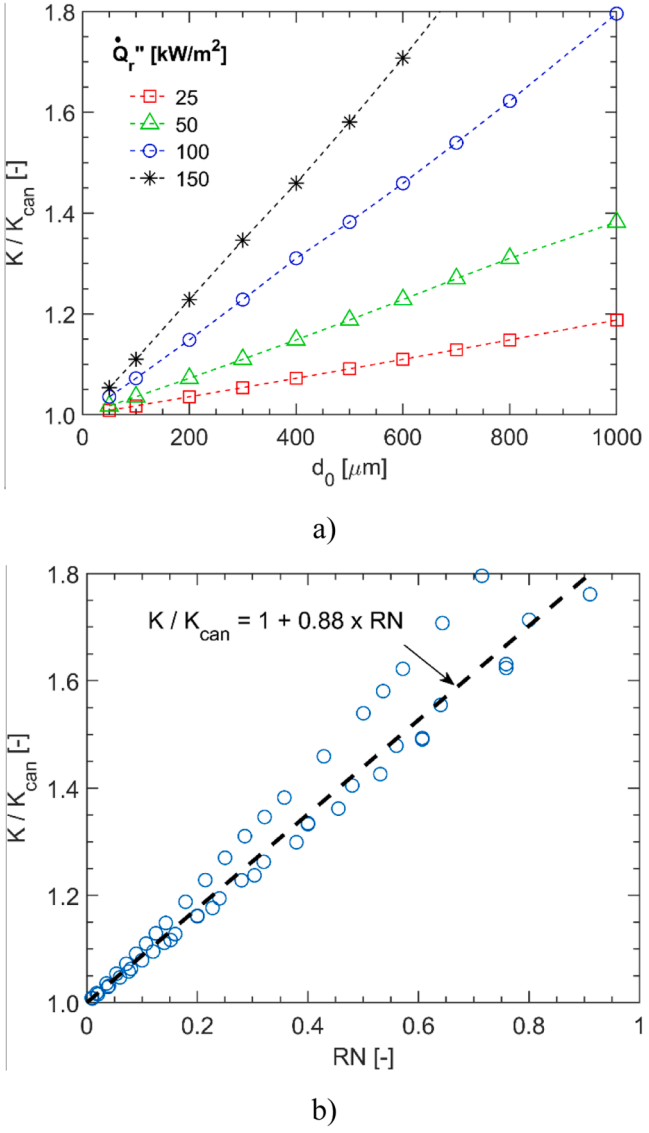

Fig. 7. (*a*) Calculated K/K_{can} for unsuspended butanol droplets as a function of d_0 for different levels of radiative heat flux ($\dot{Q}_r^{''}$) at T_g = 1400 K, Ω=4π, $\bar{E}_a$ = 0.75. (*b*) Calculated K/K_{can} vs. *RN* for a wide range of conditions: butanol and glycerol, T_g = 700 - 1400 K, d_0=50 – 1000 μm, $\dot{Q}_r^{''}$ =25 - 150 kW/m^2, Ω=4π, $\bar{E}_a$ = 0.75.

shows the variation of K/K_{can} versus *RN* for a wide range of test conditions (butanol/glycerol, T_g=700 - 1400 K, d_0=50 - 1000 μm, $\dot{Q}_r^{''}$ =25 - 150 kW/m^2). A clear correlation and, furthermore, a good linearity can be observed for the whole range explored, with slight differences when the fuel and T_g are changed. Again, the simplifications applied to obtain an *RN* based on global characteristic parameters are the cause for these differences. For instance, it should be noted that *RN* is defined in Eq. (15) based on the instantaneous droplet diameter, d_d. This implies a continuously-changing *RN* for each test case, whereas in Fig. 7b a single representative *RN* is assigned to each simulation based on its initial droplet size, d_0. The evaluation of properties can also cause some slight differences when modifying the fuel or the gas temperature. All the required gas properties are estimated based on the one-third rule proposed by Sparrow and Gregg [38], assuming that the droplet surface is at T_b. Overall, a calibration factor of 0.88 provides the best fit for the whole set of data (see the linear fitting in Fig. 7b).

Regarding the effect of forced convection on the deviation of the droplet evaporation rate from the canonical case, Fig. 8a presents the model results for a range of test conditions (d_0=50 - 1000 μm, v_g = 0.25 - 1 m/s). As expected, the relevance of forced convection increases with d_0 and v_g, since these parameters increase *Re* (and, therefore, also *Nu*). These cases, along with additional simulations changing the fuel (butanol/glycerol) and T_g (700 - 1400 K) are presented in Fig. 8b, where a clear linear correlation is found between K/K_{can} and *CN*. In this case, these results were to be expected, since *CN* is just a derivation of the Nusselt number for the droplet, and the dependence of the evaporation rate with *Nu* is well established [20]. Even though *Nu* is expected to provide a good estimate for convective effects, a coefficient of 0.54 is obtained, ascribed to the use of the initial diameter in CN and the fact that Stefan flow is neglected in this order-of-magnitude analysis.

5.2. *Analysis based on experimental data*

This section intends to evaluate the impact of the different artifacts for isolated droplet evaporation experiments, assessing also the ability of the proposed dimensionless numbers to accurately capture this impact for a wide range of experimental conditions. To that end, Fig. 9 shows

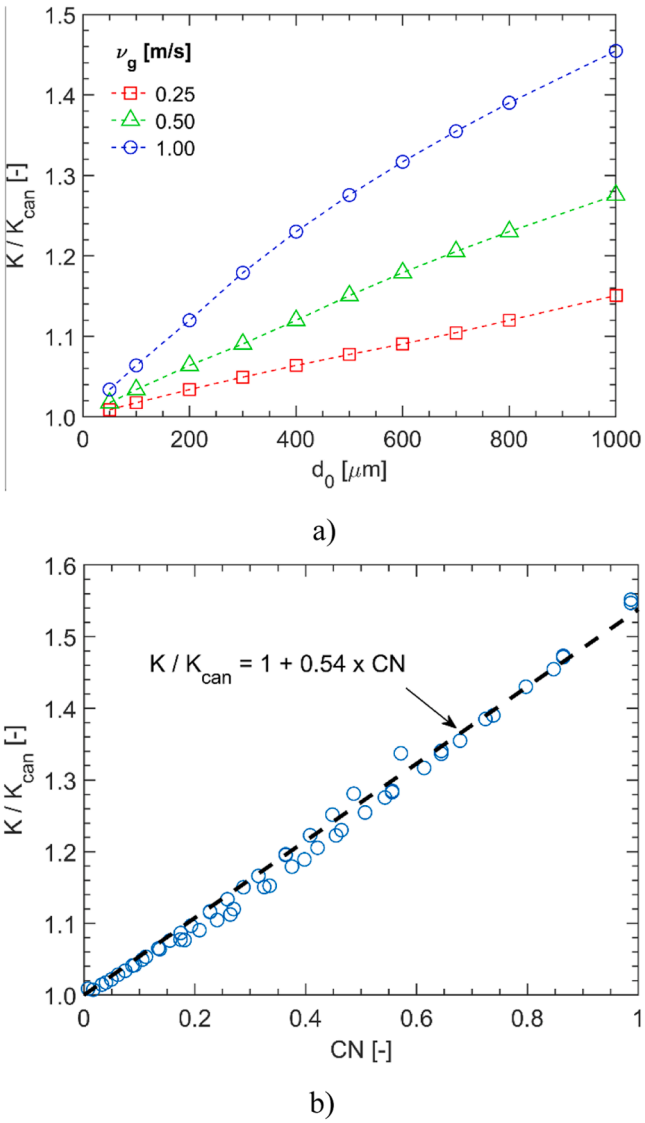

Fig. 8. (*a*) Calculated K/K_{can} for unsuspended butanol droplets as a function of d_0 for different gas velocities at T_g = 1400 K. (*b*) Calculated K/K_{can} vs. *CN* for a wide range of conditions: butanol and glycerol, T_g =700 - 1400 K, v_g =0.25 - 1 m/s, d_0 =50–1000 μm.

the isolated droplet evaporation results obtained at the SDF setup for a total of 225 cases, including different fiber arrangements, fuels, droplet sizes, etc. (results already introduced and discussed in Section 3), as well as the unsuspended free-falling droplet experiments obtained at DCF (reported in [22]).

As discussed before, some of the results from the SDF setup display clear signs of experimental artifacts, with K_{exp}/K_{can} values strongly depending on the fiber arrangement as well as on the initial droplet size. The experimental data with the lowest deviation from the canonical, artifacts-free case corresponds to very thin fibers (d_f =11 - 15 μm) of low-conductivity material (Al/Si/B and SiC) and small droplets (d_0 ~ 400 μm). This combination simultaneously reduces the non-desired additional heat transfer mechanisms to a point where K_{exp}/K_{can} ~ 1.10. On the contrary, more conductive fiber arrangements (higher k_f and/or larger fiber cross-section) in combination with small droplets can result in large errors in the measured evaporation rate, up to ~100 %, as compared to the canonical condition. Fig. 9 only shows the cases with a smooth evaporation process, removing the experiments where internal bubbling or puffing events were detected (see Fig. 4), with even larger errors in K. In contrast with the SDF results, experimental data obtained at the DCF setup display much smaller deviations from the canonical evaporation rate (~3 %). This is ascribed to the absence of the suspension medium, as well as to the low radiation absorption and weak convective effects arising from the very small droplet sizes used in these experiments.

For experimental data, it is not possible to isolate the different heat transfer modes, as it has been done in the previous section with model results, to evaluate the existence of defined trends with respect to the different dimensionless numbers. Hence, a defined functional form is needed to combine *FN, RN* and *CN*. The idealized additive relationship given by Eq. (8) will be used for that purpose and is applied in Fig. 10, where all the K_{exp}/K_{can} values shown in Fig. 9 are plotted against (*FN*+*RN*+*CN*). As in the previous section, all properties required to calculate those dimensionless numbers are evaluated by following the 1/3 rule [38] and assuming a droplet surface temperature equal to the fuel's boiling point.

Despite the widely different values and trends observed in Fig. 9, the data points in Fig. 10 become clearly grouped and display a well-defined linear tendency in this representation against the proposed dimensionless numbers. The largest deviations are obtained for glycerol droplets supported on a quartz filament, as discussed below. Moreover, the trend depicted by the data in Fig. 10 almost coincides with Eq. (8), obtained under the simplifying assumption of direct superposition of the various heat transfer modes.

As discussed before, the experimental evaporation rates obtained in

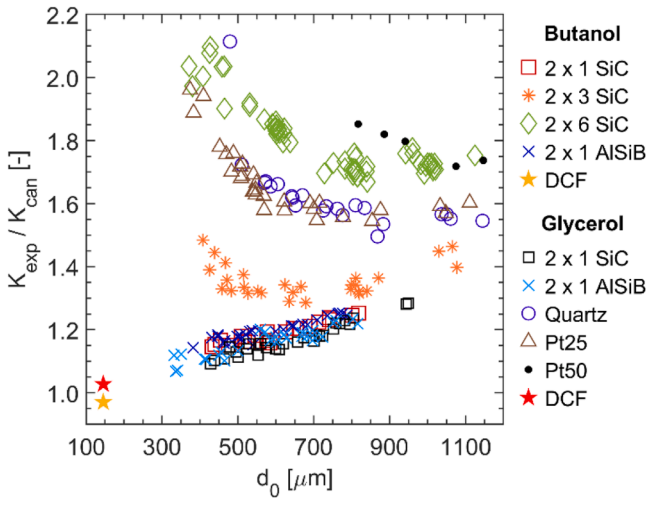

Fig. 9. K_{exp}/K_{can} vs. d_0 for different fuels and fiber arrangements.

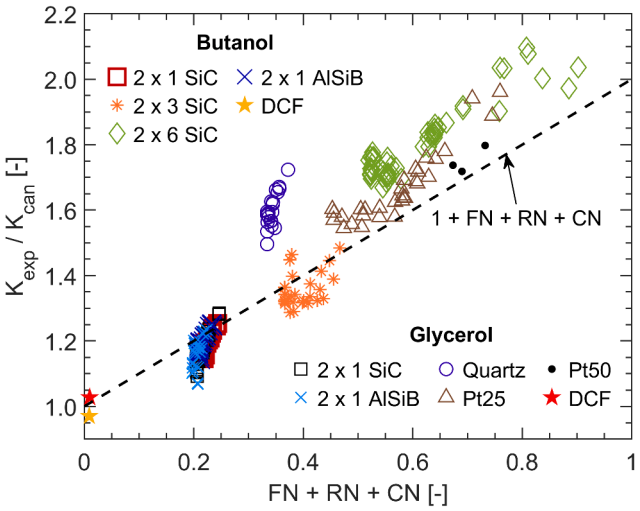

Fig. 10. K_{exp}/K_{can} vs. (*FN*+*RN*+*CN*), for SDF and DCF experimental results. The dashed line represents Eq. (8).

the fiber-free DCF setup show negligible deviations from the canonical values, in accordance with the very small values estimated for their cumulative dimensionless numbers. The SDF tests cover a much wider range of *FN*+*RN*+*CN* values (namely, between 0.2 and 0.9), which translates into substantially different K_{exp}/K_{can} values, in agreement with Eq. (8). This good alignment of the experimental data is believed to clearly support the validity of the proposed approach, as well as the ability of the dimensionless numbers to capture the shifts in droplet evaporation rate caused by these artifacts (at least for the range explored in Fig. 10). Here it is worth noting that the simulations in Figs. 6c, 7b and 8b provided with linear fitting equations, which can be used to improve the agreement of the experimental data with Eq. (8). Namely, K_{exp}/K_{can} could be plotted against $(1 + f_{cd}\,\mathrm{FN} + f_{rd}\,\mathrm{RN} + f_{cn}\,\mathrm{CN})$, being $f_{cd} = 1.21$, $f_{rd} = 0.88$ and $f_{cn} = 0.54$ correction factors obtained from the aforementioned linear regressions. However, in view of the quite good agreement in Fig. 10, the use of these correction factors was deemed unnecessary.

Among the various fiber arrangements presented in Fig. 10, the cases using a quartz fiber show the largest deviations from the predicted linear behavior. This discrepancy is hypothesized to stem from the larger diameter of the quartz fibers (100 μm) and the smaller droplet-to-fiber diameter ratio since, as discussed before, the proposed simplified approach's validity would only apply for purely 1D temperature profiles along the filament and, hence, is more suitable for thin fibers. Therefore, although these data are included in the plot, they are not a good reference to evaluate the quality of the agreement with dimensionless numbers.

Published studies from other authors have been thoroughly revised to identify experimental data that could be analyzed in the framework of the proposed approach. Several data sets have been selected, corresponding to conditions significantly different from those presented above and, at the same time, providing all data required to evaluate K_{exp} and K_{can} as well as the corresponding *FN, RN* and *CN*. Results from [4,6,23] are presented in Fig. 11 along with the already discussed SDF and DCF data, adding therefore results for a different fuel (heptane), vaporizing at significantly lower environmental temperatures (471 and 750 K). The experiments of Nomura et al. [6] are known to be affected by fiber conduction effects and the absorption of thermal radiation. Yang and Wong quantified in [23] these effects and provided a valuable analysis on the calculation of radiative absorption by the droplet. The geometric optics method and a simplified effective surface absorptance approach yielded identical results when the effective absorptance ($\bar{E}_a$) was set as 0.93 [23]. Using this approach, they modelled in [23] the

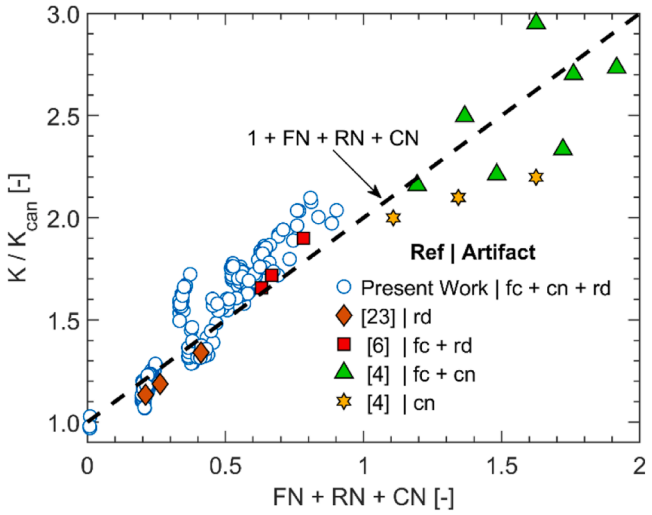

Fig. 11. K/K_{can} vs. (FN+RN+CN), for data from different sources, including own results and published works [4,6,23]. Relevant heat transfer modes affecting the different data sets are indicated as fc=fiber conduction, rd=radiation, cn=convection. The dashed line represents Eq. (8).

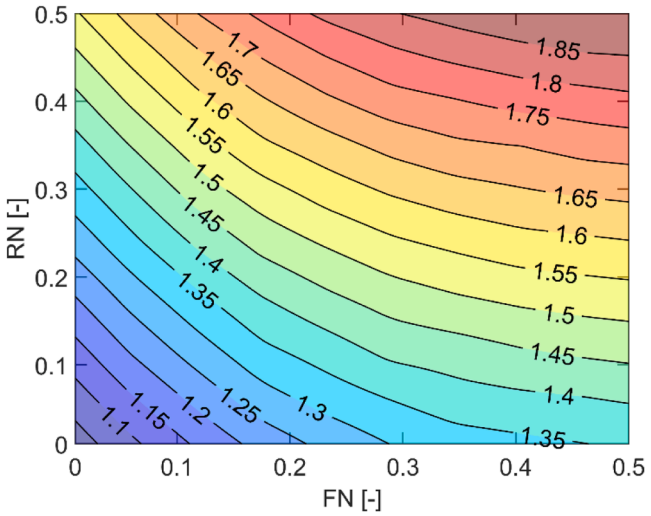

Fig. 12. K/K_{can} as a function of FN and RN, as predicted by the evaporation model.

droplet evaporation curves from microgravity experiments conducted by Nomura et al. [6], considering: a) the absence of both fiber conduction and radiation absorption (i.e., canonical case without artifacts), b) including only radiation absorption, and c) including both radiation absorption and fiber conduction (i.e., reproducing the full experiment reported in [6]). The latter two cases have been included to Fig. 11 for the three ambience temperatures explored in [6,23], yielding a remarkably good agreement with the proposed Eq. (8). The relevance of radiation becomes evident, with an increase in the droplet evaporation rate of 13, 19 and 34 % solely due to this artifact (for T_g= 471, 555 and 741 K, respectively). If fiber conduction through the 150 μm quartz filament is added, this deviation increases to 66, 72 and 90 %.

A second set of data is obtained from [4], in this case, exploring the fiber conduction and forced convection effects. Due to the specific experimental setup used, radiative heating can be considered to be negligible, and therefore, a droplet evaporation model accounting only for the additional effects of fiber conduction and convection was able to reproduce the experiments. Model calculations allow to separate both effects, since in [4] the droplet evaporation curves predicted for a no-fiber case were added, along with those accounting for different quartz fiber sizes. These two cases can be discerned in Fig. 11, where the effect of forced convection becomes apparent for the rather big-sized droplets tested in [4] (700 and 1000 μm). Namely, an enhancement of 96 % can be ascribed to this effect for a 1000 μm droplet vaporizing at 750 K. If a fiber is added (50, 150, 300 μm), this deviation increases to 112, 145 and 190 %, respectively. Again, all these cases align quite well with the linear correlation proposed in Eq. (8), further supporting the use of these dimensionless numbers to estimate the deviations in droplet evaporation rate due to experimental artifacts.

As it can be observed from the reported experimental data, the occurrence of several artifacts usually takes place simultaneously, so that the separate effect of each artifact can only be discerned either by applying some simplifying assumptions or by using evaporation models. For suspended, stationary droplet tests at high temperatures, the effects of fiber conduction and radiative heating are, arguably, the most relevant ones and their combined effect can be estimated based on model predictions. Fig. 12 shows the values of K/K_{can} predicted with the model described in Section 2.2 as a function of FN and RN, for moderate deviations from canonical conditions (both FN and RN below 0.5). This plot can be used as a two-entry chart where the input values of both dimensionless numbers would provide an estimation for the enhancement in droplet evaporation rate due to these artifacts. Iso-lines in the low FN/RN region are straight lines, as predicted by Eq. (8). Larger departures from canonical conditions result in increased curvature of the isolines, due to the non-additive nature of the different heat transfer modes. The model can account for this behavior, as long as the configuration can be reasonably assumed as 1-D, and Fig. 12 can provide better estimates than Eq. (8) for the combination of conduction and radiation artifacts. If convective effects are not negligible, its contribution could be reasonably estimated by adding 0.54 × CN (see Fig. 8b) to calculate the total deviation in K due to experimental artifacts.

In summary, the magnitude of errors with respect to evaporation rates in a canonical configuration (i.e., only $\dot{Q}_{gc}$) varies with the particular experimental conditions. Actually, all real-world tests are affected to some extent by the discussed artifacts, which can be estimated from the reported experimental and model results (e.g., Figs. 11 and 12). Nevertheless, rather small deviations can be attained by suitably selecting test conditions, targeting the set of parameters (d_0, d_f, k_f, $\dot{Q}_r''$, Re, etc.) that reduce the dimensionless numbers FN (Eq. (13)), RN (Eq. (15)) and CN (Eq. (16)). Based on these correlations, the most favorable situations are those using unsuspended droplets or very thin and non-conductive supporting fibers, low-radiative environments and small convective effects (ideally, quiescent atmosphere in microgravity). These conditions would reduce the cumulative value of FN, RN and CN, limiting therefore the value of ΔK, according to Eqs. (7) and (8).

6. Conclusions

This work presents a comprehensive investigation into the impact of different experimental artifacts on the evaporation and combustion behavior of fuel droplets. Specifically, the effect of the heat conduction through the support fibers, the absorption of thermal radiation and external convective effects are addressed. The onset of these effects can be considered to be ubiquitous in most droplet evaporation experiments, and therefore, most of the published literature data on droplet evaporation and combustion is, to some degree, affected by them. As reported in the literature, deviations in the droplet evaporation rate can even exceed 100 % due to these artifacts, as compared to the canonical case where the only heat-transfer mode is conduction through the gas-droplet interface ($\dot{Q}_{gc}$). Thus, the magnitude of these deviations should be assessed in order to allow a correct interpretation and utilization of the experimental results.

To that end, a theoretical analysis is performed, aiming to determine the relevant parameters and magnitudes of the different experimental artifacts. A dimensionless number is proposed for each artifact, based on

the ratio of the heat input due to the respective additional heat-transfer mode and $\dot{Q}_{gc}$. In this manner, the fiber, radiation, and convection numbers (*FN, RN* and *CN*, respectively) are formulated. For moderate values of these additional heat inputs, a linear correlation is obtained, indicating that the deviation of the droplet evaporation rate from the canonical case (K/K_{can}) can be predicted based on *FN, RN* and *CN*. Since these dimensionless numbers can be readily calculated based on the global characteristic parameters of the problem, the impact of each experimental artifact on the droplet evaporation rate can be easily estimated.

This theoretical analysis has been validated with results from both a droplet evaporation model and experiments at a drop-tube setup (DCF) and a suspended droplet facility (SDF). The use of these two rigs allows exploring a remarkably wide range of test conditions, particularly for the case of the SDF, for which a total number of 225 different experiments have been performed using two fuels (butanol, glycerol), several suspension fiber arrangements and materials, as well as initial droplet sizes (d_0 ~350–1200 μm). As a result, the extracted evaporation rates display a wide variability, with K/K_{can} ranging from ~ 1.1 to ~ 2.1, depending mainly on the size and conductivity of the support fibers, as well as on d_0. In contrast, results for the DCF display much smaller deviations from the canonical evaporation rate (K/K_{can} ~ 1.03), mainly due to the fact that unsuspended and very small droplets (145 μm) were tested. All these experimental results, along with literature data for quite different test conditions, proved the usefulness of the proposed approach and dimensionless numbers to analyze the deviations in evaporation rate due to these artifacts. Moreover, for small to moderate values of *FN, RN* and *CN*, the results depicted well-defined trends consistent with a superposition of the different heat transfer modes, so that the ratio K/K_{can} can be easily estimated as ~ (1+*FN*+*RN*+*CN*).

The occurrence and potential relevance of non-ideal effects in single droplet setups is profusely demonstrated by experimental and modeling results reported in this and other previous works. Whereas some configurations and conditions can result in very small or even negligible departures from the canonical situation (i.e., unsuspended droplets in a quiescent, non-radiative atmosphere under microgravity conditions), in other cases undesired artifacts can lead to large deviations. Namely, in some test conditions explored here the measured K doubled (K/K_{can}~2.1) the true evaporation rate for the canonical configuration normally assumed in tests on isolated droplets. Given the great importance of isolated droplet configurations as source of reference data for spray evaporation and combustion, the magnitude of these potential deviations needs to be critically assessed in order to correctly interpret and use experimental data. The analysis proposed in this work, in terms of easily calculable dimensionless numbers, is thought to provide a novel and valid framework in this regard that can be used, among others, to assess the magnitude of deviations for a particular case or to select the experimental conditions that minimize or limit the impact of the various experimental artifacts.

CRediT authorship contribution statement

Mohamad Asrardel: Conceptualization, Investigation, Methodology, Formal analysis, Writing – original draft, Writing – review & editing, Data curation. **Álvaro Muelas:** Conceptualization, Methodology, Formal analysis, Writing – original draft, Writing – review & editing, Data curation, Supervision. **Taha Poonawala:** Investigation, Methodology, Writing – review & editing, Data curation. **Javier Ballester:** Conceptualization, Methodology, Formal analysis, Writing – original draft, Writing – review & editing, Supervision, Funding acquisition.

Declaration of competing interest

The authors declare that they have no known competing financial interests or personal relationships that could have appeared to influence the work reported in this paper.

Acknowledgments

This work is a part of the research project PID2019-109747RB-I00, funded by MCIN/AEI/10.13039/501100011033. The financial support for M.A. and T.P. through the Pre-doctoral Fellowships BES-2017-080224 and PRE2020-094620, funded by MCIN/AEI and by "ESF Investing in your future", is gratefully acknowledged. The authors are also grateful to Luis Ojeda for his assistance with the experimental tasks.

Supplementary materials

Supplementary material associated with this article can be found, in the online version, at doi:10.1016/j.combustflame.2024.113384.

References

[1] L.J. Nunes, The rising threat of atmospheric CO2: a review on the causes, impacts, and mitigation strategies, Environments 10 (2023) 66.
[2] A.F. Ghoniem, Needs, resources and climate change: clean and efficient conversion technologies, Prog. Energy Combust. Sci. 37 (2011) 15–51.
[3] C. Chauveau, M. Birouk, F. Halter, I. Gökalp, An analysis of the droplet support fiber effect on the evaporation process, Int. J. Heat Mass Transf. 128 (2019) 885–891.
[4] J.R. Yang, S.C. Wong, An experimental and theoretical study of the effects of heat conduction through the support fiber on the evaporation of a droplet in a weakly convective flow, Int. J. Heat Mass Transf. 45 (2002) 4589–4598.
[5] Á. Muelas, P. Remacha, J. Ballester, Droplet combustion and sooting characteristics of UCO biodiesel, heating oil and their mixtures under realistic conditions, Combust. Flame 203 (2019) 190–203.
[6] H. Nomura, Y. Ujiie, H.J. Rath, J.I. Sato, M. Kono, Experimental study on high-pressure droplet evaporation using microgravity conditions, Symp. (Int.) Combust. 26 (1996) 1267–1273.
[7] K. Han, G. Song, X. Ma, B. Yang, An experimental and theoretical study of the effect of suspended thermocouple on the single droplet evaporation, Appl. Therm. Eng. 101 (2016) 568–575.
[8] C.T. Avedisian, Developing surrogates for liquid transportation fuels: the role of spherically symmetric droplet combustion, in: Novel Combustion Concepts for Sustainable Energy Development, 2014, pp. 379–402.
[9] T. Farouk, F. Dryer, Microgravity droplet combustion: effect of tethering fiber on burning rate and flame structure, Combust. Theory Model 15 (2011) 487–515.
[10] Y.C. Liu, T. Farouk, A.J. Savas, F.L. Dryer, C.T. Avedisian, On the spherically symmetrical combustion of methyl decanoate droplets and comparisons with detailed numerical modeling, Combust. Flame 160 (2013) 641–655.
[11] J. Wang, X. Huang, X. Qiao, D. Ju, C. Sun, Experimental study on effect of support fiber on fuel droplet vaporization at high temperatures, Fuel 268 (2020) 117407.
[12] G. Jackson, C. Avedisian, Combustion of unsupported water-in-n-heptane emulsion droplets in a convection-free environment, Int. J. Heat Mass Transf. 41 (1998) 2503–2515.
[13] H.Y. Setyawan, M. Zhu, Z. Zhang, D. Zhang, An experimental study of effect of water on ignition and combustion characteristics of single droplets of glycerol, Energy Proc 75 (2015) 578–583.
[14] H.Y. Setyawan, M. Zhu, Z. Zhang, D. Zhang, Ignition and combustion characteristics of single droplets of a crude glycerol in comparison with pure glycerol, petroleum diesel, biodiesel and ethanol, Energy 113 (2016) 153–159.
[15] C.T. Avedisian, G.S. Jackson, Soot patterns around suspended n-heptane droplet flames in a convection-free environment, J. Propul. Power 16 (2000) 974–979.
[16] B. Fang, L. Chen, G. Li, L. Wang, Multi-component droplet evaporation model incorporating the effects of non-ideality and thermal radiation, Int. J. Heat Mass Transf. 136 (2019) 962–971.
[17] W. Long, P. Yi, M. Jia, L. Feng, J. Cui, An enhanced multi-component vaporization model for high temperature and pressure conditions, Int. J. Heat Mass Transf. 90 (2015) 857–871.
[18] Y. Gan, L. Qiao, Radiation-enhanced evaporation of ethanol fuel containing suspended metal nanoparticles, Int. J. Heat Mass Transf. 55 (2012) 5777–5782.
[19] J. Yang, G. Jackson, C. Avedisian, Combustion of unsupported methanol/dodecanol mixture droplets at low gravity, Symp. (Int.) Combust. 23 (1991) 1619–1625.
[20] B. Abramzon, W.A. Sirignano, Droplet vaporization model for spray combustion calculations, Int. J. Heat Mass Transf. 32 (1989) 1605–1618.
[21] J. Chedaille, Y. Braud, Industrial Flames, Vol I: Measurements in Flames, Edward Arnold, London, U.K., 1972.
[22] Á. Muelas, J. Carpio, J. Ballester, A.L. Sánchez, F.A. Williams, Pyrolysis effects during high-temperature vaporization of alkane droplets, Combust. Flame 217 (2020) 38–47.
[23] J.R. Yang, S.C. Wong, On the discrepancies between theoretical and experimental results for microgravity droplet evaporation, Int. J. Heat Mass Transf. 44 (2001) 4433–4443.
[24] B. Abramzon, S. Sazhin, Droplet vaporization model in the presence of thermal radiation, Int. J. Heat Mass Transf. 48 (2005) 1868–1873.

[25] S. Churchill, M. Bernstein, A correlating equation for forced convection from gases and liquids to a circular cylinder in crossflow, J. Heat Transf. 99 (1977) 300–306.
[26] S.W. Churchill, H.H. Chu, Correlating equations for laminar and turbulent free convection from a horizontal cylinder, Int. J. Heat Mass Transf. 18 (1975) 1049–1053.
[27] P.J. Linstrom, W.G. Mallard, NIST Chemistry Webbook, NIST Standard Reference Database Number 69, National Institute of Standards and Technology, Gaithersburg, M.D., USA., 2001.
[28] W.M. Haynes, CRC Handbook of Chemistry and Physics, CRC Press, Boca Raton, USA, 2016.
[29] D.D. Johnson, Nextel 312 ceramic fiber from 3M, J. Coated Fabr. 10 (1981) 282–296.
[30] L. Binkele, Significance of discrete Lorenz function levels at high temperatures resulting from new metallic conductivity measurements, High Temp. High Press 18 (1986) 599–607.
[31] P.A. Strizhak, R.S. Volkov, G. Castanet, F. Lemoine, O. Rybdylova, S.S. Sazhin, Heating and evaporation of suspended water droplets: experimental studies and modelling, Int. J. Heat Mass Transf. 127 (2018) 92–106.
[32] S.S. Sazhin, Droplets and Sprays: Simple Models of Complex Processes, Springer, Switzerland, 2022.
[33] C. Verwey, M. Birouk, Experimental investigation of the effect of natural convection on the evaporation characteristics of small fuel droplets at moderately elevated temperature and pressure, Int. J. Heat Mass Transf. 118 (2018) 1046–1055.
[34] H.L.U. Rehman, J. Weiss, P. Seers, Effect of heat conduction on droplet life time and evaporation rate under forced convection at low temperatures, Exp. Therm. Fluid Sci. 72 (2016) 59–66.
[35] C.T. Avedisian, The homogeneous nucleation limits of liquids, J. Phys. Chem. Ref. Data 14 (1985) 695–729.
[36] D. Csemány, V. Józsa, Uncertainty of droplet evaporation measurements and its effect on model validation, in: 9th European Combustion Meeting, 2019, p. 6.
[37] T.L. Bergman, A.S. Lavine, F.P. Incropera, D.P. Dewitt, Fundamentals of Heat and Mass Transfer, John Wiley & Sons, N.J., USA., 2011.
[38] E. Sparrow, J. Gregg, The variable fluid-property problem in free convection, Trans. ASME. 80 (1958) 879–886.